

Models of supercoiled DNA interacting with an anchored cluster of proteins: towards a quantitative estimation of chromosomal DNA supercoiling

J.-C. Walter^{1*}, T. Lepage², J. Dorignac¹, F. Geniet¹, A. Parmeggiani^{1,4}, J. Palmeri¹, J.-Y. Bouet³ and I. Junier^{2*}

¹Laboratoire Charles Coulomb (L2C), Univ. Montpellier, CNRS, Montpellier, France.

²CNRS, Univ. Grenoble Alpes, TIMC-IMAG, Grenoble, France

³LMGM, CBI, CNRS, Univ. Toulouse, UPS, Toulouse, France. and

⁴DIMNP, CNRS, Univ. Montpellier, Montpellier, France.

We investigated the possibility to measure DNA supercoiling density (σ) along chromosomes using interaction frequencies between DNA and DNA-anchored clusters of proteins. Specifically, we show how the physics of DNA supercoiling leads, in bacteria, to the quantitative modeling of binding properties of ParB proteins around their centromere-like site, *parS*. We predict ParB clusters to be leaky, which actually hinders the precise measurement of σ . We propose avenues to circumvent this problem and present analyses demonstrating consistency between chromosomal and plasmid data.

In most bacteria, DNA is underwound. Despite its critical role for genome structuring [1] and coordination of gene expression [2], measurement of this negative supercoiling along chromosomes remains highly challenging, with both biological and physical difficulties.

Biological difficulties stem from the complex functioning of cells. For instance, a large part of supercoiling is known to be absorbed by various histone-like proteins [3]. The remaining supercoiling, which is responsible for the formation of branched plectonemic structures [4], is usually referred to as "free" or "effective" [5].

Physical difficulties are inherent to the dual nature of supercoiling. That is, in absence of topoisomerases, a topologically constrained DNA molecule, as in the case of a circular (plasmid) molecule or of a constrained linear domain [6], is characterized by a constant linking number, Lk , equal to the sum of the twist (Tw), the cumulative helicity of the molecule, plus the writhe (Wr), the global intricacy of the molecule [7]. As a consequence, supercoiling, i.e. the change of Lk with respect to Lk_0 , the value at rest, leads to changes in the mean values of both Tw and Wr . Having access to only Tw , when using e.g. DNA intercalating agents, is thus *a priori* insufficient to fully characterize the topological status associated with chromosomal loci [8]. This explains why supercoiling density, $\sigma = (Lk - Lk_0)/Lk_0$, has been estimated quantitatively using plasmid reporters only, since their compaction level can be quantitatively assessed *in vitro* – see [9] for an exception, although the chromosomal measurement is global, not local. Note, in this regard, that a genetic recombination-based system sensitive to the tightness of plectonemes has been developed to address variations of supercoiling density along the chromosome [10, 11]. The quantitative estimation of σ yet remains problematic because the method can only be calibrated *in vitro* [10].

Here, we investigated the possibility to measure chromosomal effective supercoiling density using DNA binding properties of the centromere-binding protein ParB from the ParABS active system of DNA segregation. It

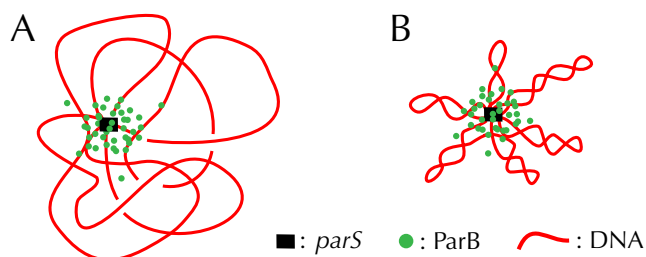


FIG. 1. *Stochastic binding model*. When DNA enters the high concentration region of the *parS*-anchored cluster of ParB, cross-linking with ParB occurs with high probability during the ChIP-seq protocol. Compared to relaxed DNA (A), supercoiling DNA (B) tends to increase DNA compaction and, hence, cross-linking with DNA loci far from *parS*.

has indeed been argued that the capture by chromatin immuno-precipitation sequencing (ChIP-seq) of the binding of ParB onto DNA in the vicinity of its specific binding site (*parS*) is driven by stochastic binding involving DNA looping properties [12] (Fig. 1). More precisely, ParB proteins have been shown to cluster inside a cage anchored at *parS* [12, 13]. In this context, only a process bringing DNA loci inside the cage/cluster can explain the slow decrease of the ParB binding profile as the genomic distance to *parS* increases (black curve in Fig. 2C) – see SI in [12] and [14] for a detailed discussion about previously proposed mechanisms.

Knowing that supercoiling properties strongly influence DNA looping properties, here we assess whether a quantitative reproduction of the non-specific ParB binding profile in the vicinity of *parS* is possible using a realistic model of bacterial DNA, *with no other free parameter than σ* . By doing so, we provide novel insights into the physical properties of ParB clusters and the structural properties of long (i.e. ≥ 30 kb) supercoiled DNA molecules. We also show the consistency between chromosomal and plasmid measurements.

Stochastic binding model. ChIP-seq detection of DNA-bound proteins involves sub-nm cross-linking be-

tween DNA and proteins [15]. In this context, we surmise that the non-specific ParB binding profile results from "collisions" between DNA and the ParB proteins located in the *parS*-anchored cluster (Fig. 1). That is, we suppose that, apart at *parS*, the timescale for ParB to unbind DNA is much smaller than the timescale for DNA to diffuse away from the location where binding occurs (instantaneous unbinding hypothesis). In this context, the modeled non-specific ParB binding profile, $B(s)$, reads [12]:

$$B(s) = \int 4\pi r^2 P_s(r) C(r) dr. \quad (1)$$

$P_s(r)$ is akin to DNA looping properties: it stands for the equilibrium probability distribution function to find a DNA locus at a genomic distance s of *parS* located in the spheric calotte of radius r centered in *parS*. For simplicity, here we neglect effects coming from the interaction between DNA and the cluster such that $P_s(r)$ is computed by considering an isolated DNA chain.

$C(r)$ stands for the probability to find a ParB protein at distance r of *parS*. Although its exact shape is still not known (see below for predictions), we have $C(r=0) = 1$ by definition of the strong binding of ParB to *parS*. The full width at half maximum of the cluster (ω_{exp} such as $C(\omega_{exp}/2) = 0.5$) has also been measured experimentally using high-resolution fluorescent microscopy [16], leading to $\omega_{exp} = 37 \pm 5$ nm.

Self-avoiding rod-like chain model of DNA. We consider a realistic 30 bp resolution polymer model of bacterial DNA, the self-avoiding rod-like chain (sRLC) model [4] (detailed simulation procedure in [17]). Specifically, DNA is modeled as a discrete chain of 10.2 nm long (30 bp of B-DNA) articulated hard-core cylinders, with radius $r_e = 2$ nm reflecting the short-range electrostatic repulsions of DNA for *in vivo* salt conditions [18]. The chain is iteratively deformed using crankshaft elementary motions with Metropolis-Hastings transition rates, under the condition that it does not cross itself. To that end, each articulating site is associated with bending and torsional energies such that the resulting persistence length, $\ell_p = 50$ nm, and torsional length, $C = 86$ nm, are typical of B-DNA for *in vivo* salt conditions [18].

Here, we discuss results obtained with a 30 kb long chain by making σ vary from 0 to -0.08 slowly enough so that chain statistical properties are insensitive to the associated speed (see Fig. S1 and simulation details in Supplementary Information). Simulated conformations are thus expected to reflect thermodynamic equilibrium, even at low values of σ where plectonemes are tight. We further checked that our results did not depend significantly on the length of the chain by performing additional simulations of 60 kb long chains (Fig. S2). Note, here, that motivations to work with $\sigma \geq -0.08$ are both biological and physical: in the worst case of topoisomerase mutants, the total supercoiling density in *E. coli* has been shown to remain above -0.08 [5], while recent work has

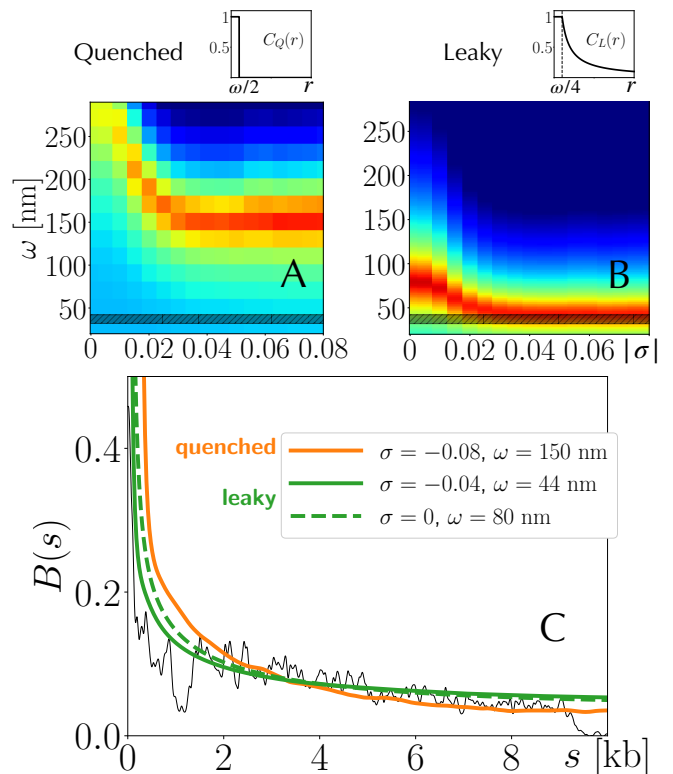


FIG. 2. *Capturing chromosomal binding profiles.* (A)(B): root mean squared deviation between modeled binding profiles (smooth curves in panel C) and ChIP-seq chromosomal data (black curve in panel C) – the redder the pixel, the smaller the deviation (arbitrary scale). The horizontal dark band indicates $\omega_{exp} (= 37 \text{ nm} \pm 5 \text{ nm})$. Best models with quenched clusters imply a large cluster ($\omega_{best} = 150$ nm, orange curve in panel C). In contrast, best models with leaky clusters imply cluster sizes very close to microscopic data when $\sigma \lesssim -0.04$ (see green curves in panel C). In this regime, all best models indeed correspond to $\omega_{best} = 44$ nm.

revealed the existence of a transition toward a hyper-branched regime occurring at $\sigma \simeq -0.08$ [19], which is beyond the scope of our discussion.

Leaky vs quenched cluster. Having in hand the corresponding $P_s(r)$ for $\sigma \in [-0.08, 0]$, we consider two extreme cases for ParB clusters: a quenched cluster defined by $C_Q(r) = \theta(\omega_{exp}/2 - r)$ (Fig. 2A) and a leaky cluster defined by $C_L(r) = \theta(\omega_{exp}/4 - r) + \frac{r_L}{r} \theta(r - \omega_{exp}/4)$ (Fig. 2B), with θ the Heaviside function – for both types, the full width at half maximum is equal to ω_{exp} . The quenched cluster mimics a very dense cluster with a sharp boundary at $r = \omega_{exp}/2$. The leaky cluster also contains a dense part, but up to $r_L = \omega_{exp}/4$. Beyond, we consider that ParB presence results from a diffusion process in the presence of a continuous source located at $r = r_L$ and we further constrain $C_L(r)$ to be continuous.

We computed binding profiles for σ ranging in $[-0.08, 0]$ and for values of the full width at half maximum of the clusters, ω , between 10 nm and 300 nm. We

compared them with profiles obtained in *E. coli* by inserting *parS* along the chromosome (black curve in Fig. 2C) – only one side of the chromosome is analyzed as the other side is distorted by the presence of strong promoter regions [13]. In this experiment, 10 *parS* sites interspersed by 43 base pairs, as found in the natural *parS* region, were inserted at *xylE* [13]. A careful analysis of the binding properties among these multiple *parS* sites actually revealed significant variations of the ChIP-seq signal, which was thus normalized with respect to the maximum value. The origin of the curvilinear abscissa s is set right at the edge of the most extreme *parS* site. Note, finally, that experiments were performed with a saturated concentration of ParB [13], which justifies to use $C_{Q/L}(r) = 1$ below $r_{Q/L}$.

We are interested in explaining the global shape of the binding profile as it is expected to reflect generic polymer physics principles. To that end, we quantify the explanatory power of each model by reporting the root mean square deviation with respect to the experimental binding profile for $s \in [1.5 \text{ kb}, 9 \text{ kb}]$. Both the lower and upper bounds at 1.5 kb and 9 kb, respectively, are used to avoid specific, reproducible distortions of the signal associated with the presence of gene promoters and sites for regulatory DNA proteins [13].

In this context, we find that both quenched and leaky clusters can capture experimental data rather well (Fig. 2A). However, best quenched models are found at $\omega_{best} = 150 \text{ nm}$ (Fig. 2B), which is much larger than ω_{exp} . In contrast, best leaky models are found at $\omega_{best} = 44 \text{ nm}$ when $\sigma \lesssim -0.04$ (Fig. 2C and green plain curve in Fig. 2A), compared to the dashed curve obtained for $\sigma = 0$. That is, they explain data in the physiological relevant situation of the plectonemic regime. They also solve an issue associated with the previous version of the stochastic binding model where supercoiling was neglected and where DNA persistence length had to be set to a very small value to “mimic” corresponding compaction [12].

Interestingly, compared to chromosomal *parS* data, ParB binding profiles in the vicinity of a *parS* located on a plasmid (100 kb long F-plasmid [13]) show less distortion (Fig. 3) – just as for the chromosome, only one side of the plasmid is analyzed as the other side is distorted by binding sites for a replication initiator [12]. In this context, best leaky models lead to similar model parameters ($\omega_{best} = 42 \text{ nm}$ when $\sigma \lesssim -0.04$), while providing an even better match with data below $s = 4 \text{ kb}$ and above $s = 9 \text{ kb}$ (Fig. 3).

σ -sensitive probes for strong supercoiling.

While leaky models with experimentally relevant ω capture experimental data rather well, resulting binding profiles are almost indistinguishable for $\sigma \in [-0.08, -0.04]$ (see e.g. Fig. 3). This lack of sensitivity is concomitant with a poor variation of global structural features in the plectonemic regime, such as the radius of gyration (blue

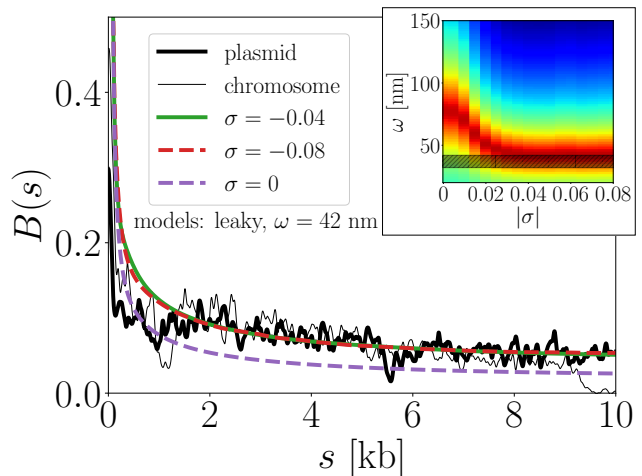


FIG. 3. *Plasmid profiles.* Experimentally, plasmid binding profiles (thick black curve) are less distorted than chromosomal profiles (thin black curve). Models in this context capture even better experimental data, both below $\sim 4 \text{ kb}$ and above 9 kb . Inset: same as Fig. 2C but using plasmid experimental data, with $\omega_{best} = 42 \text{ nm}$.

curve in Fig. S3). Note that, in contrast, branching properties can vary significantly in this regime [1, 19]. For instance, we find that the number of plectonemic branches reaches a maximum at $\sigma \simeq -0.05$ (orange curve in Fig. S3), in accord with previous analyses with smaller molecules [1] and with a minimum value of the hydrodynamic radius for 10 kb long plasmids [1, 19, 20].

A natural question, then, is whether it is possible to build a probe that is sensitive to variations of σ for strong supercoiling. Interestingly, we have found a possible solution consisting of a system that senses intertwining properties of plectonemes, in the spirit of the $\gamma\delta$ recombination system [10]. To that matter, one would need a quenched (instead of a leaky) cluster that is small enough such that the binding properties of proteins is sensitive to the diameter and pitch of plectonemes [21, 22]. For instance, our simulations reveal a strong sensitivity of $P_s(r)$, at the kb genomic scale for s , with respect to *all values of σ* for spatial distances r on the order of 10 nm (inset of Fig. 4). One can verify, then, that a quenched cluster with $\omega = 20 \text{ nm}$ provides well-distinct binding profiles for $\sigma \in [-0.08, 0]$ (Fig. 4). Notice the much smaller values of $B(s)$ in this case, compared e.g. to results in Figs. 2 and 3. ParB ChIP-seq experiments can nevertheless report very low binding frequencies as demonstrated by titration assays [13].

Discussion and perspectives. First of all, let us note that the large 150 nm width required by models with a quenched cluster to match experimental data is actually compatible with the first report of ω_{exp} [12]. In this work, cells and clusters were not fixed so that measurement was hindered by cluster diffusion. This hence

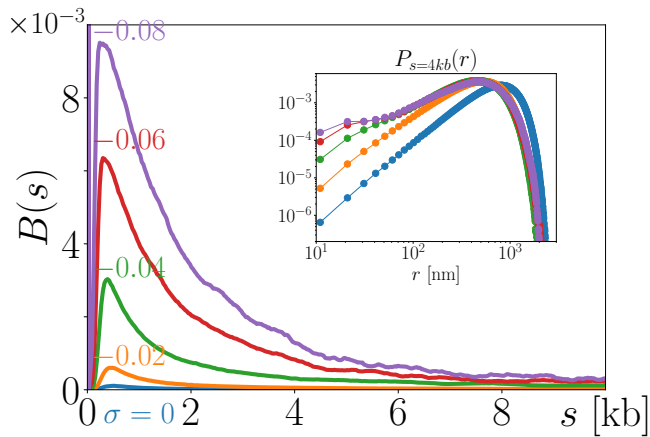


FIG. 4. *Designing a probe to discriminate a wide range of supercoiling densities.* In the context of a poorly extended quenched cluster ($\omega = 20$ nm), binding profiles are well separated for values of $\sigma \in [-0.08, 0]$ as soon as the variation is on the order of 0.01, which would thus provide a reasonable precision of supercoiling measurement. Inset: in the plectonemic regime (green, red and purple curves), the spatial distribution of distances between loci only differ significantly at small distances, that is, at distances that reflect plectonemic inter-twining of the DNA molecule.

suggests the existence of a "mapping" between leaky and diffusive quenched clusters, which we aim to explore in a future more detailed version of the model. Along this line, one would like to have an explicit modeling of ParB nucleation and diffusion properties to develop a detailed model of the interactions between ParB and DNA using e.g. molecular dynamics approaches. In particular, the discrepancy between experimental and modeling profiles below ~ 1 kb (Fig. 3) might be the result of our approximation of neglecting hard-core interactions between ParB proteins and DNA. Finally, at large scales, cellular confinement of DNA should be included in the model. We note, nevertheless, that a complete picture would require studying the melting of a plectonemic tree-like structure at the chromosome scale, which is currently beyond the capacities of numerical simulations.

From an instrumental viewpoint, while our framework does not involve any adjustable parameter, binding profiles in the presence of leaky clusters cannot be used to precisely determine the effective supercoiling density σ (Fig. 3). They can "only" provide an upper bound (-0.04), which corresponds to the onset of the plectonemic regime. As shown above, a supercoiling-sensitive probe could then be provided by a small quenched cluster that can "sense" physical properties of plectonemes, in the spirit of existing genetic recombination-based probes [10, 11]. Yet, compared to these "biological" probes, our "physical" probe should be less sensitive to molecular environment as it is based on generic (polymer) physics properties. For instance, recombination-

based systems depend on (slow) enzymatic recombinase reactions, whose quantitative modeling, to the best of our knowledge, has remained elusive. In practice, while genetic design of such ParB clusters could be tricky, transcription factors could provide an efficient system. These proteins have indeed the capacity of binding both cognate DNA sites strongly and other DNA sites non-specifically with (short) millisecond residence times [23]. They could also be used in fusion with a DNA methyltransferase so that to generate methylation (instead of binding) profiles without the need of crosslinking stages [24]. Finally, a sensitive system would require to have DNA devoid as much as possible of interfering biological elements, such as gene promoters, which distort the utilizable physical signal.

Acknowledgements. We thank Daniel Jost for useful suggestions. JCW was supported by a "Modélisation pour le Vivant" CNRS Grant (CoilChrom). J.Y.B. is supported by an AO80Prime (Numacoiled) CNRS grant. I.J. was supported by an ATIP-Avenir grant (Centre National de la Recherche Scientifique).

* correspondence should be sent to:
 jean-charles.walter@umontpellier.fr
 ivan.junier@univ-grenoble-alpes.fr

- [1] A. Vologodskii and N. Cozzarelli, Annual Review of Biophysics and Biomolecular Structure **23**, 609 (1994).
- [2] C. J. Dorman and M. J. Dorman, Biophysical reviews **8**, 89 (2016).
- [3] A. Travers and G. Muskhelishvili, Current Opinion in Genetics & Development **15**, 507 (2005).
- [4] A. V. Vologodskii, S. D. Levene, K. V. Klenin, M. Frank-Kamenetskii, and N. R. Cozzarelli, Journal of Molecular Biology **227**, 1224 (1992).
- [5] J. B. Bliska and N. R. Cozzarelli, Journal of molecular biology **194**, 205 (1987).
- [6] L. F. Liu and J. C. Wang, PNAS **84**, 7024 (1987).
- [7] J. H. White, American Journal of Mathematics **91**, 693 (1969).
- [8] A. Lal, A. Dhar, A. Trostel, F. Kouzine, A. S. N. Seshasayee, and S. Adhya, Nature communications **7**, 11055 (2016).
- [9] R. R. Sinden, J. O. Carlson, and D. E. Pettijohn, Cell **21**, 773 (1980).
- [10] B. M. Booker, S. Deng, and N. P. Higgins, Molecular Microbiology **78**, 1348 (2010).
- [11] N. S. Rovinskiy, A. A. Agbleke, O. N. Chesnokova, and N. P. Higgins, Microorganisms **7** (2019).
- [12] A. Sanchez, D. I. Cattoni, J.-C. Walter, J. Rech, A. Parmeggiani, M. Nollmann, and J.-Y. Bouet, Cell Systems **1**, 163 (2015).
- [13] R. E. Debaugny, A. Sanchez, J. Rech, D. Labourdette, J. Dorniac, F. Geniet, J. Palmeri, A. Parmeggiani, F. Boudsocq, V. Anton Leberre, J.-C. Walter, and J.-Y. Bouet, Molecular Systems Biology **14**, e8516 (2018).

- [14] J.-C. Walter, N.-O. Walliser, G. David, J. Dorignac, F. Geniet, J. Palmeri, A. Parmeggiani, N. S. Wingreen, and C. P. Broedersz, *New Journal of Physics* **20**, 035002 (2018).
- [15] E. A. Hoffman, B. L. Frey, L. M. Smith, and D. T. Auble, *The Journal of biological chemistry* **290**, 26404 (2015).
- [16] B. Guilhas, J. C. Walter, J. Rech, G. David, N. O. Walliser, J. Palmeri, C. Mathieu-Demaziere, A. Parmeggiani, J. Y. Bouet, A. L. Gall, and M. Nöllmann, *bioRxiv* (2020), <http://dx.doi.org/10.1101/791368>.
- [17] T. Lepage and I. Junier, *Methods in molecular biology* (Clifton, N.J.) **1624**, 323 (2017).
- [18] T. Lepage, F. Képès, and I. Junier, *Biophysical Journal* **109**, 135 (2015).
- [19] B. A. Krajina and A. J. Spakowitz, *Biophysical Journal* **111**, 1339 (2016).
- [20] J. C. Wang, *Journal of molecular biology* **87**, 797 (1974).
- [21] J. Marko and E. Siggia, *Physical Review E* **52**, 2912 (1995).
- [22] C. Barde, N. Destainville, and M. Manghi, *Physical Review E* **97**, 032412 (2018).
- [23] J. Elf, G. Li, and X. S. Xie, *Science* **316**, 1191 (2007).
- [24] J. Redolfi, Y. Zhan, C. Valdes, M. Kryzhanovska, I. M. Guerreiro, V. Iesmantavicius, G. Tiana, T. Pollex, J. Kind, S. Smallwood, W. d. Laat, and L. Giorgetti, *bioRxiv*.

Supplementary information:
Models of supercoiled DNA interacting with an anchored cluster of proteins:
towards a quantitative estimation of chromosomal DNA supercoiling

J.-C. Walter, T. Lepage, J. Dorignac, F. Geniet, A. Parmeggiani, J. Palmeri, J.-Y. Bouet and I. Junier

CONTENTS

I. Simulation protocol	1
II. Supplementary Figures	2

I. SIMULATION PROTOCOL

Starting from a random conformation obtained at $\sigma = 0$, a simulation run consists in starting with $\sigma = 0$ and repeating the following steps up to $\sigma = -0.08$:

1. Perform \mathcal{N} sweeps at constant σ (cf below for the parameters and quantities associated with the Monte-Carlo method)
2. Decrease σ by 0.005
3. Goto 1

As a result, we have statistics for 17 values of σ that are regularly spaced between -0.08 and 0 . The associated supercoiling rate, per sweep, of σ variation is hence given by $v = -0.005/\mathcal{N}$, with $\mathcal{N} = 5 \times 10^5$ and $\mathcal{N} = 1.6 \times 10^7$ for the quickest and slowest simulations, respectively – in the following, for clarity, we normalize v such that $v = 1$ for the quickest simulations (Fig. S1). Note that, in our simulations, a maximum of $M = 100$ cylinders can be rotated during a crankshaft rotation. Simulations being performed with a resolution of 30 bp per cylinder, a 30 kb long chain is made of $N = 1000$ cylinders such that a sweep corresponds to $N/M = 10$ Monte-Carlo steps. As a result, the slowest simulations with $\mathcal{N} = 1.6 \times 10^7$ corresponds to $\mathcal{N}_{MC} = 1.6 \times 10^8$ Monte-Carlo steps, so that one simulation run for the slowest case involves $17 \times 1.6 \times 10^8 = 2.72 \times 10^9$ Monte-Carlo steps.

For each simulation run, for further statistical analysis we have considered 2500 conformations between the $(N/2)^{th}$ sweep (mid-total number of sweeps) and the N^{th} sweep (last sweep). For instance, Fig. S1 shows, for each supercoiling rate, the mean value of the radius of gyration as a function of σ together with the standard error of the mean. The latter is computed using the variance of the mean of the radii of gyration obtained from the 20 different simulation runs, i.e. $\sqrt{\text{var}(R_g)/19}$ where $\text{var}(R_g)$ is that variance. Fig. S1 shows in particular that for rates smaller than $v = 1/8$, results may be considered independent of v . As a consequence, results of the main text, such as $P_s(r)$, have been obtained using 60 independent simulation runs coming from the three slowest rates ($v = 1/8, 1/16, 1/32$).

II. SUPPLEMENTARY FIGURES

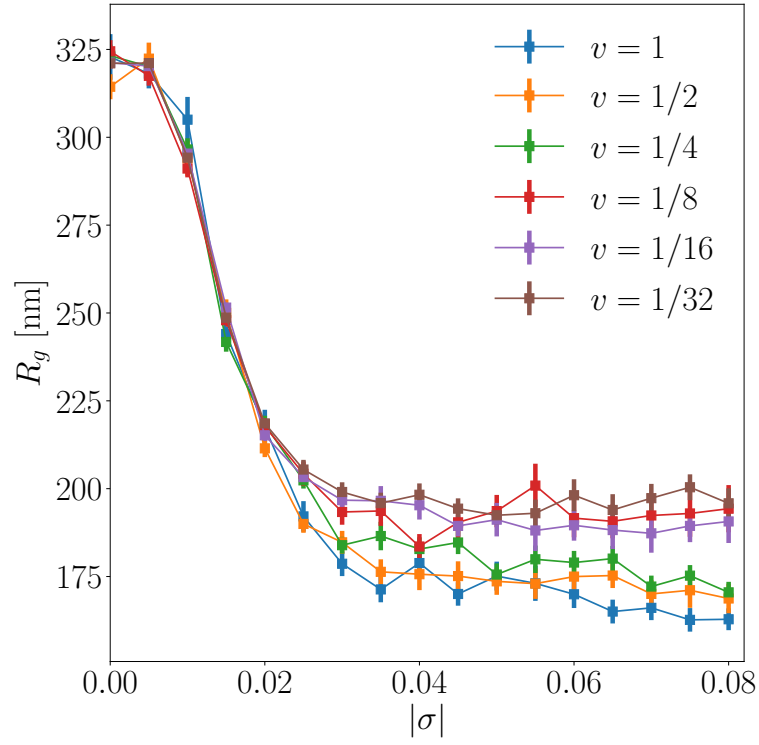


FIG. S1. *Sensitivity of results with respect to supercoiling rates.* In this plot, a point corresponds to the mean value of the radius of gyration obtained at a given σ for a specific supercoiling rate v (see explanations for the protocol). The error bars correspond to the standard error of the mean computed over 20 different simulation runs.

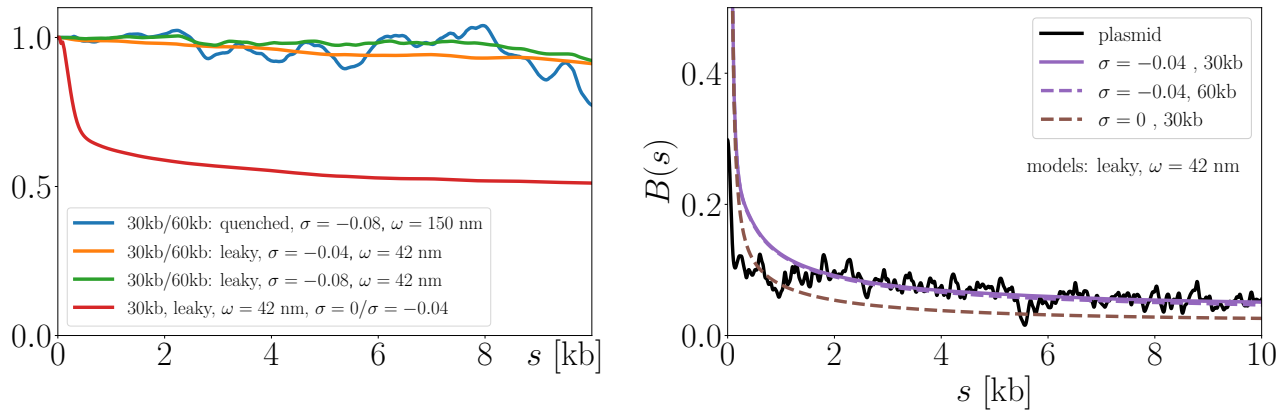


FIG. S2. *Below 10 kb, only slight differences exist between binding profiles obtained with 30 kb long molecules and those obtained with 60 kb long molecules. Left panel:* the blue, orange and green curves stand for the ratio of binding profiles between 30 kb and 60 kb long molecules obtained with different combinations of σ , ω and type of cluster. Red curve: ratio of binding profiles for a 30 kb long molecule with a leaky cluster and $\omega = 42$ nm between $\sigma = 0$ and $\sigma = -0.04$. **Right panel:** We report the binding profiles used to compute the orange and red curves on the left panel to demonstrate that differences between 30 kb and 60 kb long molecules are indeed not significant from the viewpoint of experimental data. By contrast, the difference is significative between $\sigma = 0$ (brown dashed curve) and $\sigma = -0.04$ (purple curves).

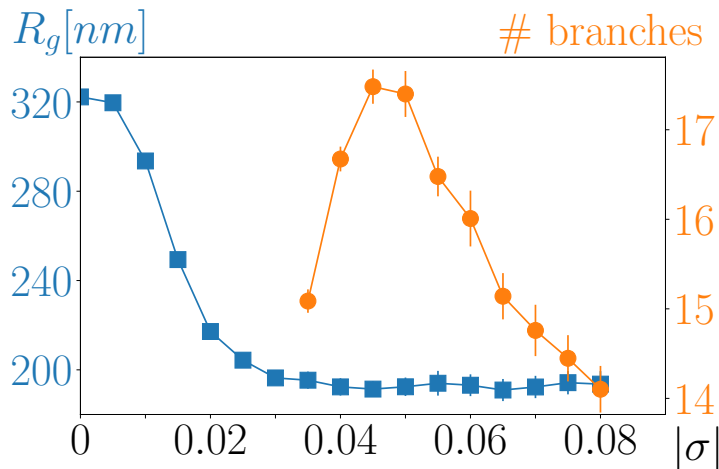


FIG. S3. *Radius of gyration and number of branches as a function of $|\sigma|$. The radius of gyration reaches a plateau at $|\sigma| \simeq 0.04$. The number of branches is non-monotonous, reaching a maximum at $|\sigma| \simeq -0.05$.*